Sintering mechanism and grain growth in CaCu 3 Ti 4 O 12 ceramics

G. Riquet, S. Marinel, Y. Bréard, C. Harnois

Sintering mechanism and grain growth in $CaCu_3Ti_4O_{12}$ ceramics

Guillaume RIQUET [1]*, Sylvain MARINEL [1], Yohann BREARD [1], Christelle HARNOIS [1]

[1]: Laboratoire de Cristallographie et Science des Matériaux, Normandie Univ, ENSICAEN, UNICAEN, CNRS, CRISMAT, 14000 Caen, France

*: Corresponding author

E-mail address: guillaume.riquet@ensicaen.fr

Postal address : Laboratoire CRISMAT, 6 Boulevard du Maréchal Juin, 14050 CAEN Cedex 4, France

Abstract

In this work, a study of the densification of $CaCu_3Ti_4O_{12}$ (CCTO) ceramics during conventional sintering process is presented. Dilatometric study was conducted in detail to find out which diffusion mechanism is responsible for densification. Based on the shrinkage curves, it was shown that densification is mostly controlled by grain boundary diffusion. The microstructure evolution of CCTO during conventional sintering was studied through the sintering trajectory, which corresponds to a unique relationship between grain size and density. According to SEM analysis, it was shown that abnormal grain growth takes place for samples sintered at high temperature stage with density > 80% of the theoretical density. Finally, the Master Sintering Curve (MSC) method was also used to characterize the densification process of CCTO and estimate the apparent sintering activation energy (Q=730 $kJmol^{-1}$).

Keywords: $CaCu_3Ti_4O_{12}$; Sintering ; Microstructure ; Grain growth

I. Introduction

In the last years, the research of materials having high dielectric constant with good temperature stability has raised significant attention because of their interest in many potential applications. The cubic double distorted perovskite like structure of $CaCu_3Ti_4O_{12}$ (CCTO) (SG Im3; a = 7.393 Å), which contains square-planar Cu atoms on A site inducing the tilt of TiO_6 octahedra, has attracted much attention [1-2]. In terms of dielectric properties, CCTO ceramic has a high relative dielectric permittivity at room temperature of $\varepsilon_r \sim 10^5$ at 1 kHz with good temperature stability on a wide temperature range [100K, 400K] and no phase transition. The IBLC model has often been reported to explain this apparent high dielectric permittivity in CCTO ceramics. This model suggests the presence of an Internal Barrier Layer Capacitor, consisting of semiconducting grains separated by thin insulating grain boundaries [3-4]. In addition, below 100K, a drastic decrease of the permittivity down to 100 has been reported [5-6].

A literature survey has clearly reported that CCTO dielectric properties are strongly correlated to its microstructure, therefore it is necessary to pay attention to the processing conditions from which microstructure highly depends. Recently, Riquet et al. [7] has successfully synthesized CCTO by conventional and microwave heating conducting to different initial average grain sizes, i.e. 1µm and 400 nm, respectively. After conventional sintering of the two powders in air at 1050 °C for 2h, they observed similar microstructures with large grains up to 30 µm and inter/intra porosity, indicating that abnormal grain growth occurs during sintering. Fang et al. [8] have also observed discontinuous grain growth for different samples sintered from 1035°C to 1065°C, and that for different sintering times in air. In their experimental conditions, grain size was remaining practically constant for heat treatment duration lower than 8h at 1035°C or lower than 3h at 1065°C. According to the literature, this sudden grain growth is correlated to the apparition of a Cu-rich intergranular phase at the high temperature stage [9]. These microstructures changes may have an impact on the dielectric properties of CCTO. For instance, Adams et al. [10] have measured an increase of the permittivity value, measured at 10 kHz, from 9000 to 280 000 , for ceramics sintered, respectively, at 1100°C for 3h and 24h. While density for both samples were almost identical, the average grain sizes were very different i.e., 6 µm and 100 µm respectively, showing the high dependence of the permittivity of CCTO on the microstructure.

Therefore, it is well established that dielectric properties of CCTO highly depend on the sintering conditions. So far, only the presence of abnormal grain growth at high temperature stage has been reported. Nonetheless there is a lack of information regarding the sintering mechanisms involved during the overall sintering process of CCTO. Therefore, the aim of this paper is to bring new insights into the densification behavior of CCTO material during conventional sintering. Dilatometric study was conducted in detail to find out which diffusion mechanism is responsible for densification. Based on this dilatometric data, the Master Sintering Curve (MSC) was also determined. This method was originally developed by Su and Johnson [11] and is a powerful tool to predict and characterize the densification process of ceramics and to estimate the apparent sintering activation energy. Finally, the microstructure evolution of CCTO during conventional sintering was studied through the sintering trajectory. This trajectory corresponds to a unique relationship between grain size and density, being given a starting powder and one sintering process.

II. Experimental

1. *Powder synthesis and materials shaping*

The solid state synthesis of CCTO was performed using highly pure $CaCO_3$ (99,95% Alfa Aesar), CuO (99,7% Alfa Aesar) and anatase-TiO_2 (99,9% Materion) as starting materials. The precursors were mixed and grounded by ball milling during 16 min (Fritsch Pulverisette 6 planetary mill) with respect to the stoichiometry of $CaCO_3$-3CuO-4TiO_2. The mixed precursor powder was subsequently heated three times in air in a tubular furnace using the following thermal cycle: heating up to 900°C at 2.5 °C min^{-1} with a dwell of 10h. An organic binder (PVA - 1 wt%) was used to ensure a good cohesion of the compacted green samples. The CCTO powder was shaped into disks by uniaxial pressing at 5 MPa (6 mm in diameter, 6 mm thick) followed by an isostatic pressing step at 200 MPa. The binder was removed by a heat treatment in air at 400°C for 2h. The green sample density was close to 61 % of the theoretical value (5.05 g cm^{-3}).

2. *Sintering conditions and characterizations*

The samples were conventionally sintered in air at temperatures ranging from 1000°C to 1100°C with different dwell times using two different furnaces: (i) in a Thermo-Mechanical Analysis chamber (TMA) with heating and a cooling rate of 5°C min^{-1} to record the shrinkage during the heating process. (ii) In a conventional tubular furnace with a heating rate of 5°C min^{-1}, which allows quenching samples from the high temperature stage to room temperature. The samples were then quenched in air to observe the evolution of the microstructure as the sintering process progressing. For the construction of the Master Sintering Curve (MSC), seven samples were sintered using the TMA furnace at 1050°C for 2h using different heating rates: 5°C min^{-1}, 7.5°C min^{-1}, 10°C min^{-1}, 12.5°C min^{-1}, 15°C min^{-1}, 17.5°C min^{-1} and 20°C min^{-1}.

Based on these dilatometric curves and assuming isotropic shrinkage, the sample density can be calculated as a function of the temperature from the shrinkage value, by using the following equation:

$$\rho(T) = \frac{\rho_{Archi}}{(1+\frac{S_t - S_f}{h_f})^3} \quad (1)$$

where ρ(T) is the instantaneous relative density (g.cm^{-3}), ρ_{Archi} the final density measured by Archimedes's method in absolute ethanol (g.cm^{-3}), S_t the instantaneous vertical shrinkage (µm), S_f the final vertical shrinkage (µm) and h_f the final height of the sample (µm). The X-Ray Diffraction (XRD) measurements were performed on a Theta-Theta PANalyticalX'Pert Pro diffractometer with a CuKα (λ=1.54059 Å) radiation. The Rietveld method using Fullprof program was used for the structural refinement. The microstructural characterizations were carried out using a scanning electron microscope (SEM Zeiss Supra 55), equipped with an Energy Dispersive Spectroscopy (EDS) System. The average grain size was estimated by linear intercept method over 200 grains of different micrographs to ensure a good reliability. [12]

3. *Construction of the Master Sintering Curve (MSC)*

The master sintering curve is obtained by separating the sintering parameters into: (i) those related to the microstructure (ii) those related to the thermal history of the material. According to Su and Johnson [11], these parts are related to each other experimentally and the temperature dependent side can be expressed as:

$$\theta = \frac{1}{c}\int_{T_0}^{T_m} \exp(\frac{-Q}{RT})dT \qquad (2)$$

where c is the heating rate, T_0 the starting temperature, T_m the maximum reached temperature and Q the apparent activation energy for densification.

The curves of the density (ρ) versus the log(θ) parameter are constructed for each heating rate. The mean ρ=f(log(θ)) curve can be calculated, and the convergence of data is quantified through the calculation of the mean residual square obtained from the experimental data points and the mean curve. If we can find a Q value for which all ρ=f(log(θ)) curves coincide regardless the heating rates (and so that minimizes the value of the mean residual squares), then this single ρ versus θ curve is called the master sintering curve of the densification process and this particular Q value represents the apparent sintering activation energy. In such a case, the grain size is independent of thermal history and it is only a function of density.

III. Results and discussions

1. Sintering mechanisms

Figure 1 shows the XRD pattern and the SEM microstructure of the as-synthesized CCTO powder, with a narrow average particle size distribution centered at 800 nm. According to the structural refinement, apart some weak diffraction peaks characteristic of CuO (1%) and $CaTiO_3$ (1%) which are observed at extremely low amounts, all the diffraction peaks can be attributed to CCTO phase. Figure 2

represents the variation of the linear shrinkage and relative density of a CCTO sample versus temperature, for the following temperature cycle: heating up to 1100°C at 5°C min^{-1} with a dwell time of 2 hours. The relative densities were calculated using Eq (1). During solid state sintering of ceramics, several diffusion mechanisms may be involved but only volume and grain boundary diffusion cause material to migrate from inside the particles to the neck surface, resulting in material densification. To determine the dominant diffusion mechanism controlling the densification, the shrinkage equations during isothermal sintering can be used [13]. Assuming that grain growth is negligible, which is a reasonable assumption during the initial stage of sintering; the linear shrinkage equation (in isothermal condition) can be expressed as follows:

Grain boundary diffusion: $$\left(\frac{\Delta L}{L_0}\right)^3 = \left(\frac{3\delta_G D_G \gamma_{SV} \Omega}{4r^4 RT}\right).t \quad (3)$$

Volume diffusion: $$\left(\frac{\Delta L}{L_0}\right)^2 = \left(\frac{16\pi D_J \gamma_{SV} \Omega}{r^3 RT}\right).t \quad (4)$$

where ΔL is the linear shrinkage, L_0 the initial thickness of the sample, δ_G is the thickness of the grain boundary, D_G is the grain boundary diffusion coefficient, γ_{SV} represents the solid-vapor surface energy of the solid, Ω is the molar volume of the solid, D_J represents the lattice diffusion coefficient, r is the grain size, R the universal gas constant, T is the temperature and t the time. By plotting the logarithm of the shrinkage versus the logarithm of the time (in isothermal condition), a linear equation can be obtained and the slope value can be used to determine the dominant diffusion mechanism leading to densification: ½ for volume diffusion and ⅓ for grain boundary diffusion.

The experimental isothermal shrinkage curve measured at 1000°C is shown on figure 3a. The final density of the sintered sample was 73% of the theoretical value. Experimentally, the $\ln(\Delta L/L_0)=f(\ln(t))$ plot is shown in figure 3b., and represents a straight line with a slope value b=0.31 which clearly indicates that grain boundary diffusion mechanism is the dominant diffusion mechanism for densification during the CCTO initial stage of sintering. To check that no grain growth occurs during the initial stage of sintering, samples were heated (up to 4% of relative shrinkage) and quenched in air. Figure 3b also shows a SEM microstructure of CCTO at the end of the initial step of sintering, with a

density of ρ=67.9% and an average grain size of 850 nm. This confirms that grain growth is negligible during the initial stage of sintering. Otherwise, those data confirm the validity of isothermal equations previously used. For several density, the average grain size of CCTO samples was estimated and is represented in figure 4. It is shown that the grain size remains nearly constant for density ranging from 60% to 80%. As shown in figures 3b and 5(a,b,c), the average grain size slightly increases from 800-850 nm during the initial stage sintering (60-68% density range) to 1.3 µm (78.9% of density), showing that grain growth is very limited for this density values range. However, figures 4 and 5 show that exaggerated grain growth occurs beyond ρ = 80 % of the theoretical density. Figure 5g shows SEM micrograph using an AsB detector to reveal composition contrasts on the image. Coupling with EDS mapping of grains and grain boundaries in figure 6, it reveals that a Cu-rich phase is present and segregates at grain boundaries. This microstructural evolution of CCTO is consequently in good agreement with already reported abnormal grain growth phenomenon. This latter mechanism was often explained by the presence of a small amount of CuO which segregates at triple point site and grain boundaries at high temperature [8].

2. *Application of the Master Sintering Curve*

It must be kept in mind that several conditions must be fulfilled to properly use the MSC concept. First the MSC can be applied only to samples shaped with the same powder, green-body process and green density. Another assumption is that microstructural evolution depends only on density and that one diffusion mechanism dominates in the sintering process. Practically, deviations from these assumptions can be observed. As previously seen, the grain size-density trajectory has shown an abrupt grain size increasing at density >80%, indicating the initiation of the exaggerated grain growth phenomenon. Therefore, it makes sense not to include data taken in this density range in the initial MSC analysis to avoid confusion during the process of minimization of the sums of residual squares.

Different values of activation energy Q were tested, and the ρ=f(log(θ)) curves for all heating profiles were plotted using Eq. (1) and Eq. (2). The convergence of the data can be quantified through the sum of the residual squares. When the best estimate of Q is found, all the data should converge to a single curve and the mean residual squares is a minimum. The minimum was reached at ~ 730 kJ mol^{-1}, as shown in figure 7a, and represents the apparent sintering activation energy for CCTO. The resulting MSC is given (figure 7c) and shows that the ρ=f(log(θ)) curves from the different heating rates have merged onto a single curve but only over the medium density range, up to 80% of the theoretical density.

Over the range 60% - 80 % of the theoretical density, the master sintering curve was obtained and no deviation was observed. This confirms that the solid state sintering of CCTO is taking place with one dominant diffusion mechanism during the sintering process in this density range, which was found to be grain boundary diffusion. Nonetheless, the high apparent sintering activation energy, Ea = 730 kJ mol^{-1}, suggests a difficult densification of the material during the early stage of sintering. To understand this high value of the sintering activation energy, it is worthy to pay attention on the microstructure evolution between the green shaped compact (see figure 5a) and the same microstructure on the sintered compact at 1080°C with no dwell time (figure the 5c). Actually, just after synthesis, necks between particles are partially formed (see the arrow) showing that the early stage of sintering has already started ($x/r \neq 0$). After sintering at 1080°C (fig. 5.c), the x/r value has slightly increased but its value remains low, showing that the diffusion through the grain boundary is taking much energy (high value of Ea). Over this stage, the densification takes place through the sintering of the agglomerates and the homogenization of the microstructure.

Beyond 80% of the theoretical density, abnormal grain growth in CCTO occurs, which explains the clear discrepancy on figure 7c on the MSC curves. The same phenomenon has already been observed for some materials such as TiO_2-doped Al_2O_3 [11-14] for which the sintering data points do not converge for high values of density. On this study, they reported an abrupt increase of the grain size for densities higher than 95% of the theoretical value, indicating the initiation of exaggerated grain growth. A similar behavior is observed on CCTO. As the sintering temperature increases, it is shown that a Cu-

rich phase segregates at grain boundaries, as clearly observed on the figure 6. This Cu rich phase is most likely at the liquid state [15-16] during the high temperature stage as this phase seems to coat the grains. Therefore, the abnormal grain growth results from this liquid phase which promotes the dissolution-diffusion-precipitation process, known as Ostwald ripening mechanism [17]. The consequence is that small grains disappear to the benefit of very large grains. Figure 8 proposes a scheme to summarize this grain growth mechanism through the Ostwald ripening phenomenon for densities higher than 80 % of the theoretical value. This scheme also shows what is happening for density lower than this threshold value.

IV. Conclusion

In this work, the densification behavior of $CaCu_3Ti_4O_{12}$ during conventional sintering has been deeply investigated. Sintering trajectory (grain size vs density) and Master Sintering curves have been determined and can be divided in two distinct regions. From 60% to 80 % of the theoretical density, the densification mostly takes place and the grain size remains constant and close to 1.1 µm. Based on the linear shrinkage equation, it was also shown that the dominant diffusion mechanism leading to densification during the initial stage of sintering is the grain boundary diffusion. For this mechanism, the apparent sintering activation energy, determined by using the MSC model, was found to be ~730 $kJ.mol^{-1}$. This relatively high value can be correlated to the quite low variation of the sintering advancement over this sintering stage (x/r value evolution). For higher densities (>80%), grain size increases exponentially, indicating the initiation of the exaggerated grain growth due to the presence of a Cu-rich liquid phase at grain boundaries. This liquid phase promotes the dissolution-diffusion-precipitation mechanism known as Oswald Ripening phenomenon. Further investigations using transmission electron microscopy are in progress to probe the origin of the Cu-rich phase and the nanoscale compositional variations in the grain and grain boundary regions of CCTO ceramics.

Acknowledgments

The authors thank the French Ministry of Research for the financial support. The authors are also thankful to Jerome Lecourt and Christelle Bilot for their help in conducting the experimental work.

References

[1] M.A. Subramanian, D. Li, N. Duan, B.A. Reisner, A.W. Sleight, *High Dielectric Constant in $ACu_3Ti_4O_{12}$ and $ACu_3Ti_3FeO_{12}$ Phases*, J. Solid State Chem. 151 (2000) 323–325. https://doi.org/10.1006/jssc.2000.8703

[2] A.P. Ramirez, M.A. Subramanian, M. Gardel, G. Blumberg, D. Li, T. Vogt, S.M. Shapiro, *Giant dielectric constant response in a copper-titanate*, Solid State Communications 115 (2000) 217–220. https://doi.org/10.1016/S0038-1098(00)00182-4

[3] D.C. Sinclair, T.B. Adams, F.D. Morrison, A.R. West, *$CaCu_3Ti_4O_{12}$: One-step internal barrier layer capacitor*, Appl. Phys. Lett. 80 (2002) 2153–2155. https://doi.org/10.1063/1.1463211

[4] R. Schmidt, M.C. Stennett, N.C. Hyatt, J. Pokorny, J. Prado-Gonjal, M. Li, D.C. Sinclair, *Effects of sintering temperature on the internal barrier layer capacitor (IBLC) structure in $CaCu_3Ti_4O_{12}$ (CCTO) ceramics,* J. Eur. Ceram. Soc. 32 (2012) 3313–3323. https://doi.org/10.1016/j.jeurceramsoc.2012.03.040

[5] P. Lunkenheimer, R. Fichtl, S.G. Ebbinghaus, A. Loidl, *Nonintrinsic origin of the colossal dielectric constants in $CaCu_3Ti_4O_{12}$,* Phys. Rev. B 70 (2004) 172102. https://doi.org/10.1103/PhysRevB.70.172102

[6] M.C. Ferrarelli, D.C. Sinclair, A.R. West, H.A. Dabkowska, A. Dabkowski, G.M. Luke, *Comment on the origin(s) of the giant permittivity effect in $CaCu_3Ti_4O_{12}$ single crystals and ceramics,* J. Mater. Chem. 19 (2009) 5916–5919. https://doi.org/10.1039/B910871H

[7] G. Riquet, S. Marinel, Y. Breard, C. Harnois, A. Pautrat, *Direct and hybrid microwave solid state synthesis of CaCu3Ti4O12 ceramic: Microstructures and dielectric properties*, Ceram. Int. 44 (2018) 15228–15235. https://doi.org/10.1016/j.ceramint.2018.05.164

[8] T.T Fang, H.K. Shiau, *Mechanism for Developing the Boundary Barrier Layers of $CaCu_3Ti_4O_{12}$*, J. Am. Ceram. Soc. 87 (2004) 2072–2079. https://doi.org/10.1111/j.1151-2916.2004.tb06362.x

[9] K.M. Kim, J.H. Lee, K.M. Lee, D.Y. Kim, D.H. Riu, S.B. Lee, *Microstructural evolution and dielectric properties of Cu-deficient and Cu-excess $CaCu_3Ti_4O_{12}$ ceramics,* Mater. Res. Bull. 43 (2008) 284–291. https://doi.org/10.1016/j.materresbull.2007.03.014

[10] T.B. Adams, D.C. Sinclair, A.R. West, *Giant Barrier Layer Capacitance Effects in $CaCu_3Ti_4O_{12}$ Ceramics,* Adv. Mater. 14 (2002) 1321–1323. https://doi.org/10.1002/1521-4095(20020916)14:18<1321::AID-ADMA1321>3.0.CO;2-P

[11] H. Su, D.L. Johnson, *Master Sintering Curve : a practical approach to sintering*, J.Am. Ceram. Soc. 79 (1996) 3211-3217. https://doi.org/10.1111/j.1151-2916.1996.tb08097.x

[12] M.I. Mendelson, *Average grain size in polycrystalline ceramics*, J. Am. Ceram. Soc. 52 (1969) 443–446. https://doi.org/10.1111/j.1151-2916.1969.tb11975.x

[13] D. Bernache-Assollant, *Chimie-physique du frittage*, Hermès (1993)

[14] J. Wang, R. Raj, *Estimate of the activation energy for boundary diffusion from rate-controlled sintering of pure alumina and alumina doped with zirconia or titania*, J. Am. Ceram. Soc. 73 (1990) 1172-75. https://doi.org/10.1111/j.1151-2916.1990.tb05175.x

[15] W. Yuan, *Investigation on the decomposable process and the secondary liquid phase effect on the dielectric properties of $CaCu_3Ti_4O_{12}$ ceramics*, J. Phys. D: Appl. Phys. 42 (2009) 175401. https://doi.org/10.1088/0022-3727/42/17/175401

[16] T.B. Adams, D.C. Sinclair, A.R. West, *Decomposition Reactions in $CaCu_3Ti_4O_{12}$ Ceramics*, J. Am. Ceram. Soc. 89 (2006) 2833–2838. https://doi.org/10.1111/j.1551-2916.2006.01174.x

[17] N.B. Singh, A. Berghmans, M. King, D. Knuteson, J. Talvacchio, D. Kahler, M. House, B. Schreib, B. Wagner, S. McLaughlin, *Modification of interface anisotropy and its effect on microstructural evolution during ostwald ripening,* Cryst. Res. Technol. 48 (2013) 983–988. https://doi.org/10.1002/crat.201300204

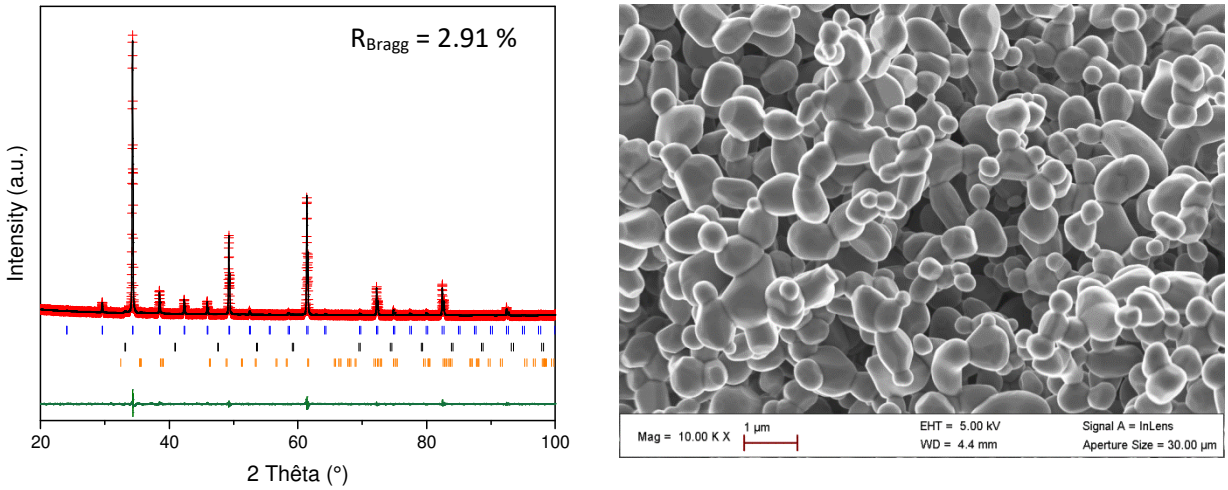

Figure 1: X-Ray diffraction patterns (λ = 1.594 Å) recorded at 300K and SEM micrographs of $CaCu_3Ti_4O_{12}$ powder obtained by conventional synthesis.

Experimental: red crosses. Calculated: black line. Difference: green line. The blue vertical bars are the positions of the reflections allowed by $CaCu_3Ti_4O_{12}$. The black set of vertical bars is correlated to the secondary phase $CaTiO_3$, while the orange vertical bars indicate the reflections allowed by the phase CuO.

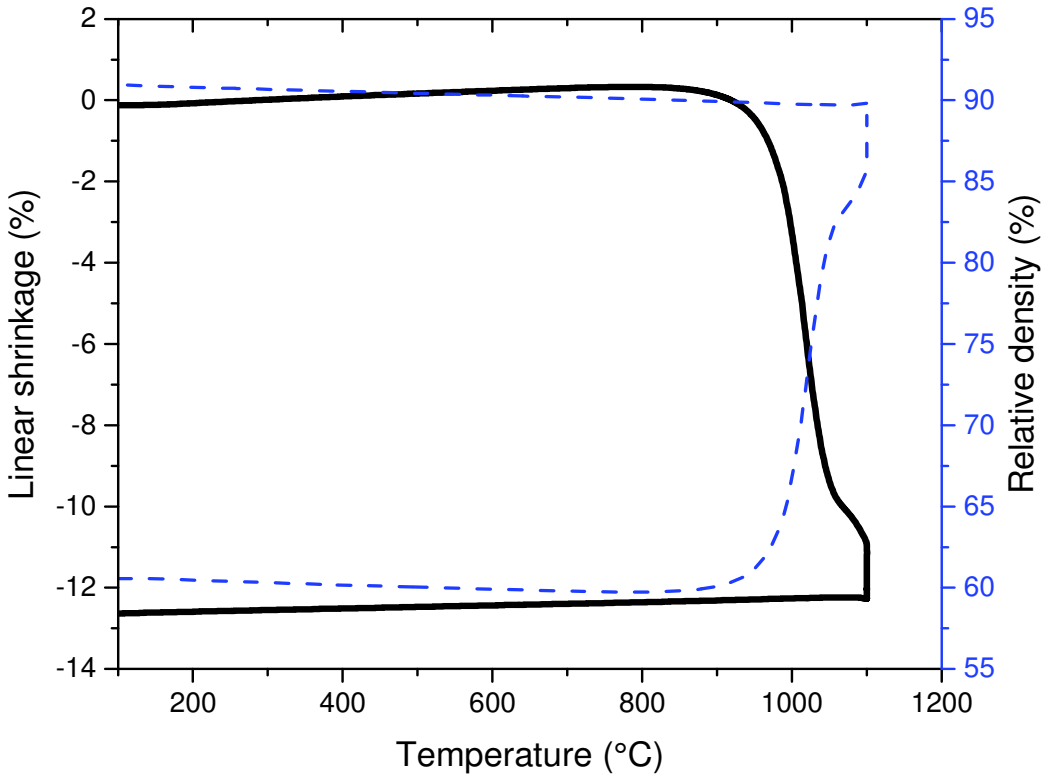

Figure 2: Linear shrinkage (black) and relative density (dash) curves of CCTO sample.

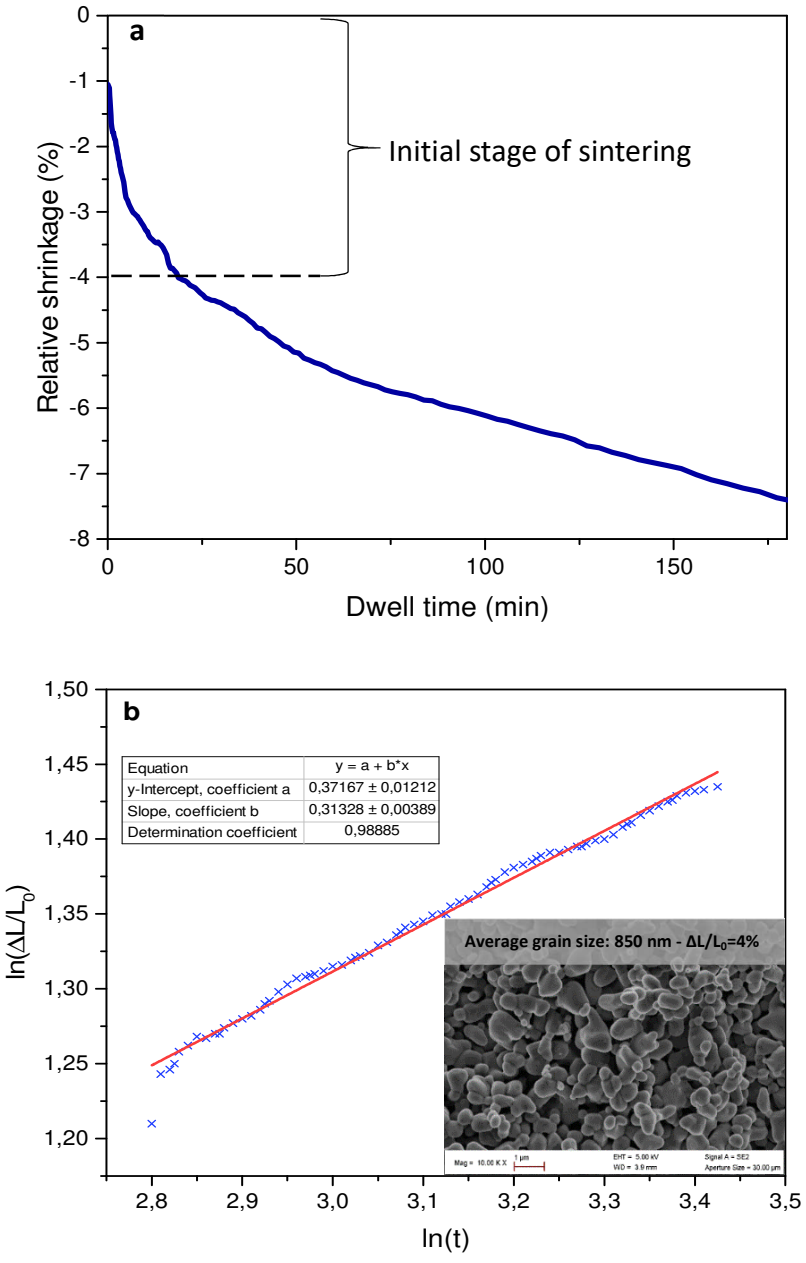

Figure 3: (a) Relative shrinkage vs dwell time at 1000°C - (b) Linear shrinkage equation during initial stage of sintering and SEM micrographs of CCTO sample at the end of the initial stage sintering.

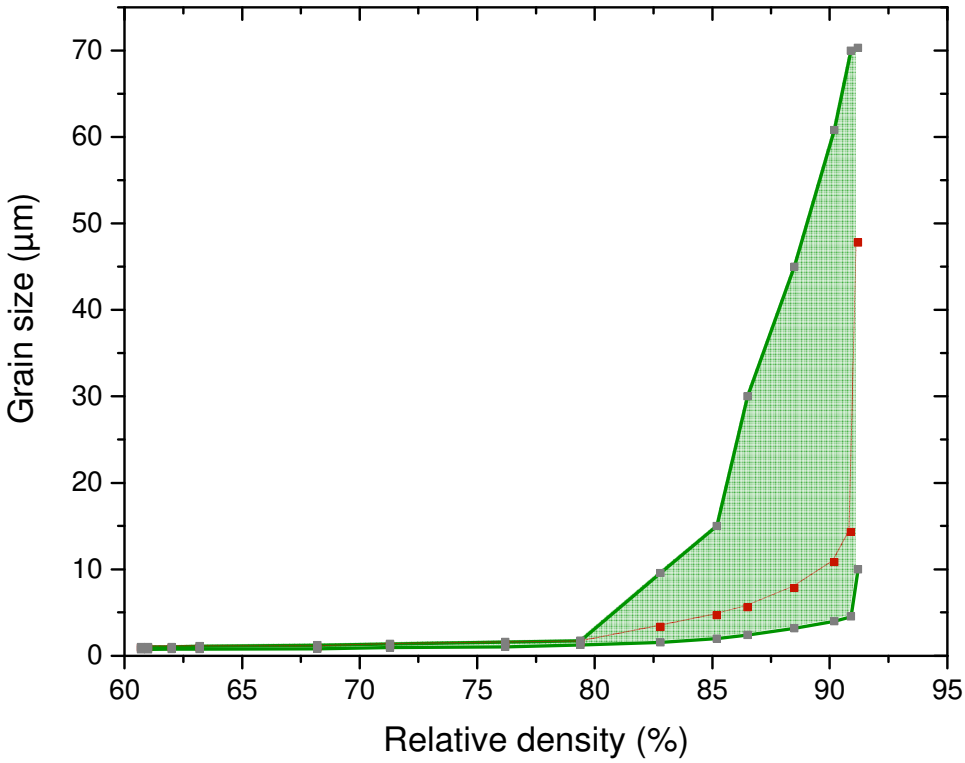

Figure 4: Grain size vs Relative density trajectory of conventionally sintered CCTO

Red curve represents the average grain size of the different samples. Gray points represent minimum and maximum grain sizes.

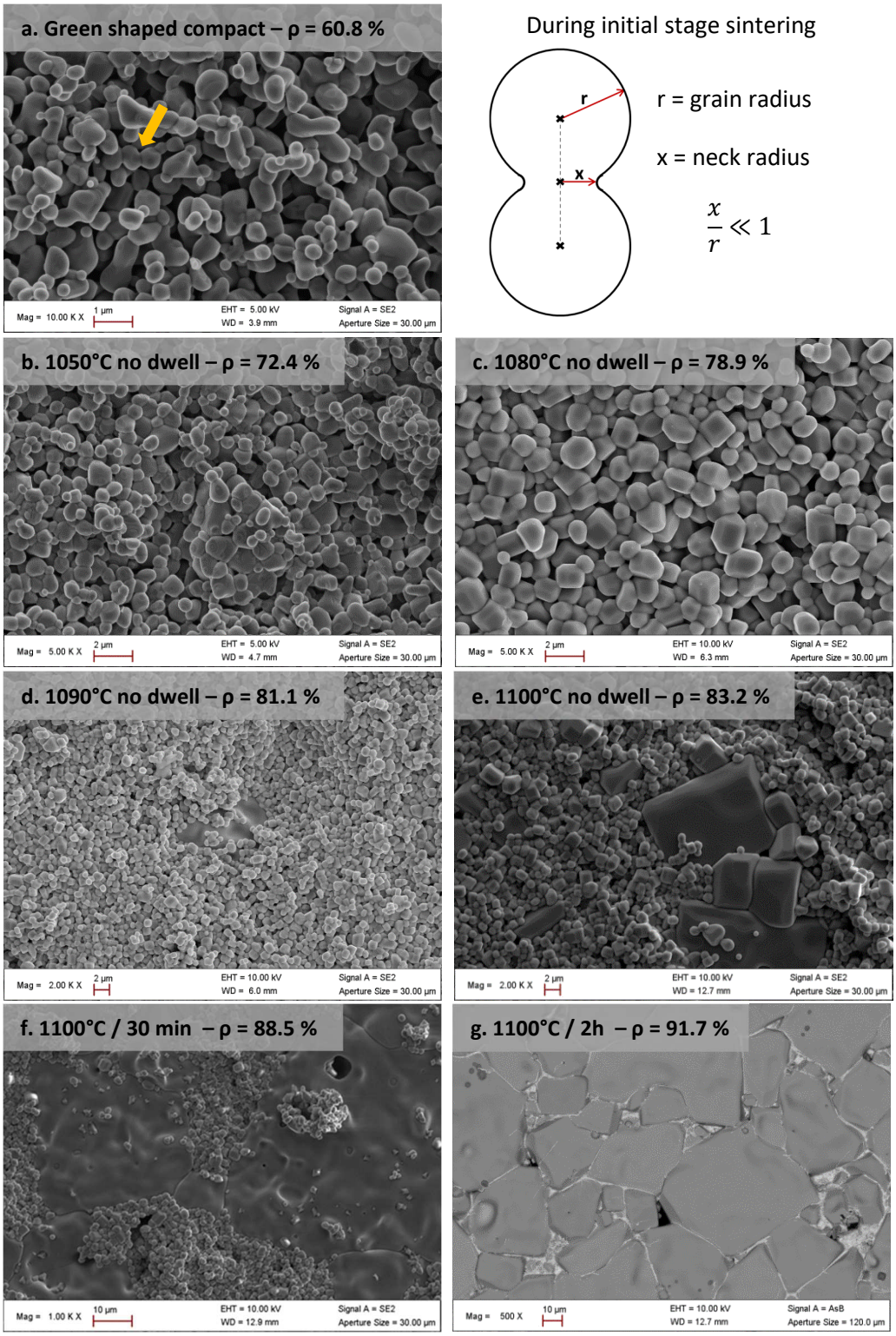

Figure 5: SEM micrographs of sintered samples at different densities (a) ρ=60.8 % (b) ρ=72.4 % (c) ρ=78.9 % (d) ρ=81.1 % (e) ρ=83.2 % (f) ρ=88.5 % (g) ρ=91.7 %

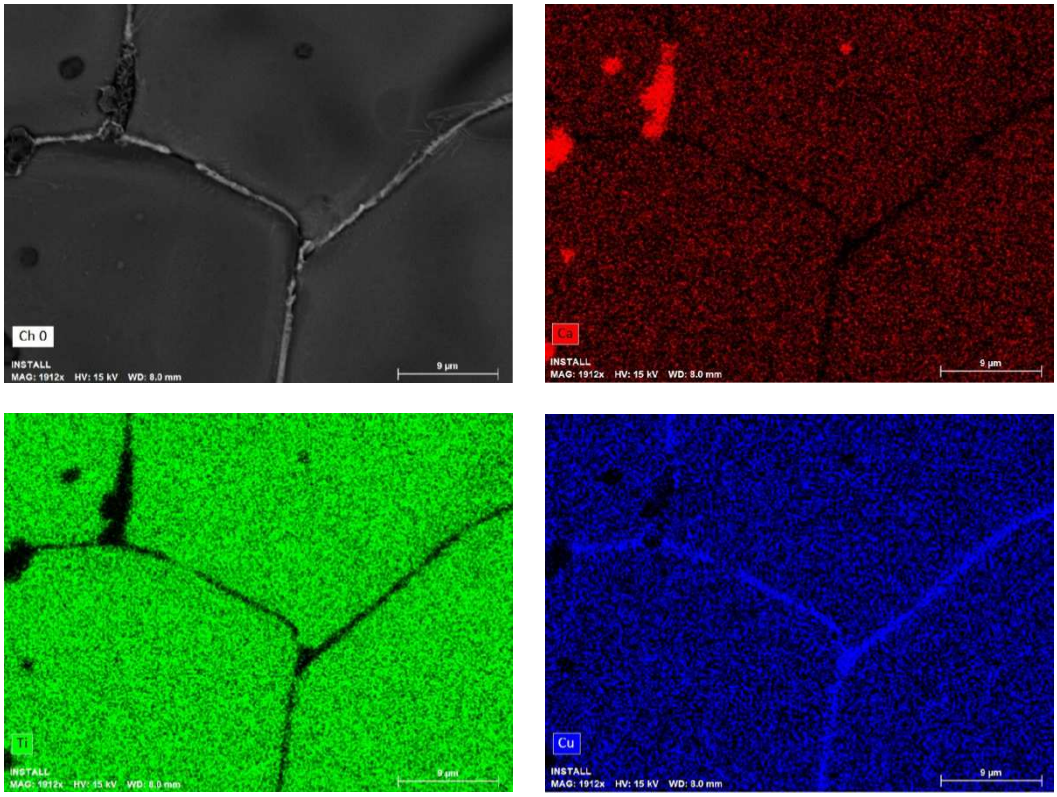

Figure 6: EDS mapping of CCTO sample sintered at 1100°C for 2h.

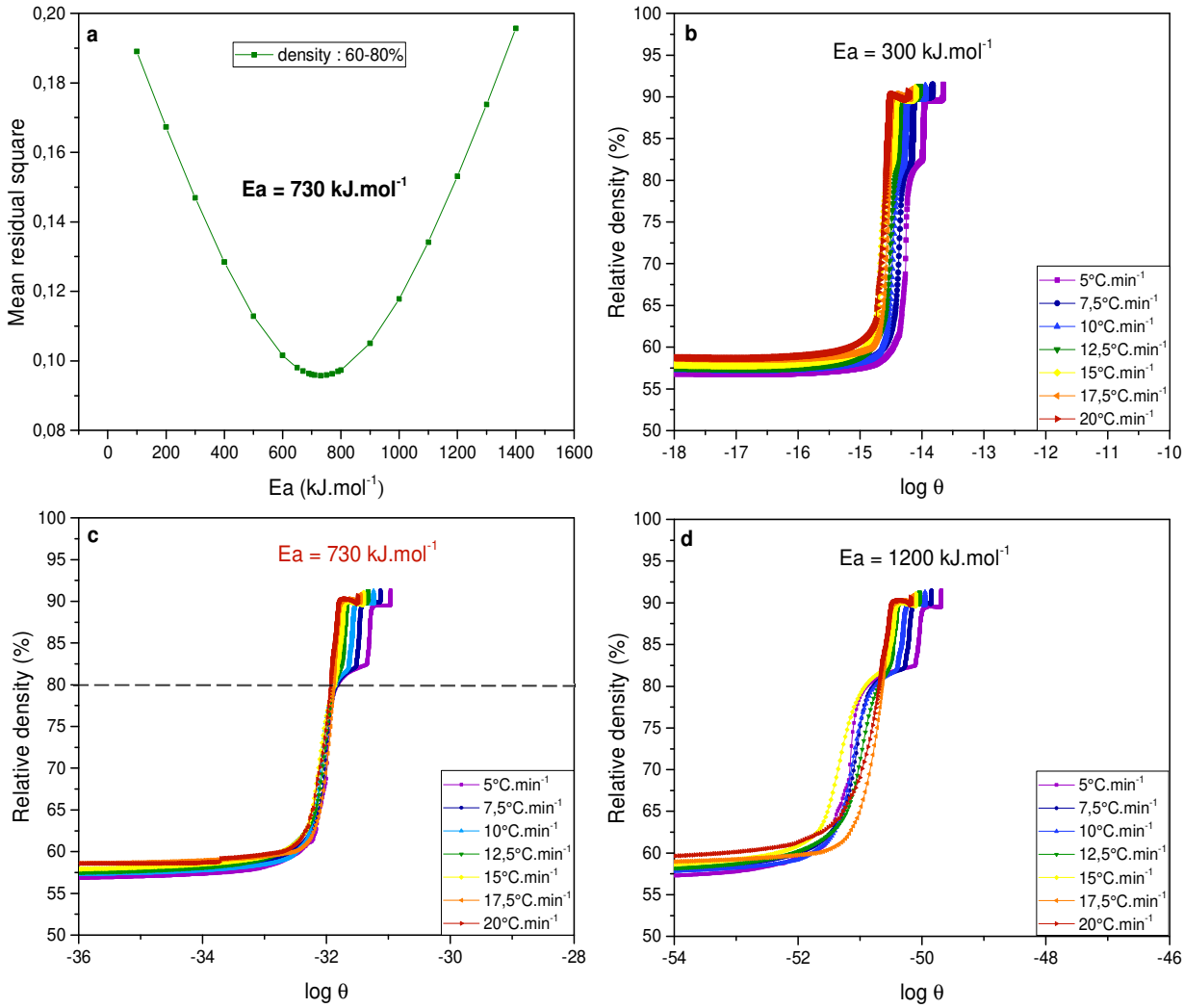

Figure 7: (a) Estimation of the apparent sintering activation energy.
Application of the "Master Sintering Curve" model using different activation energies:
(b) 300 kJ mol^{-1} (c) 730 kJ mol^{-1} (d) 1200 kJ mol^{-1}.

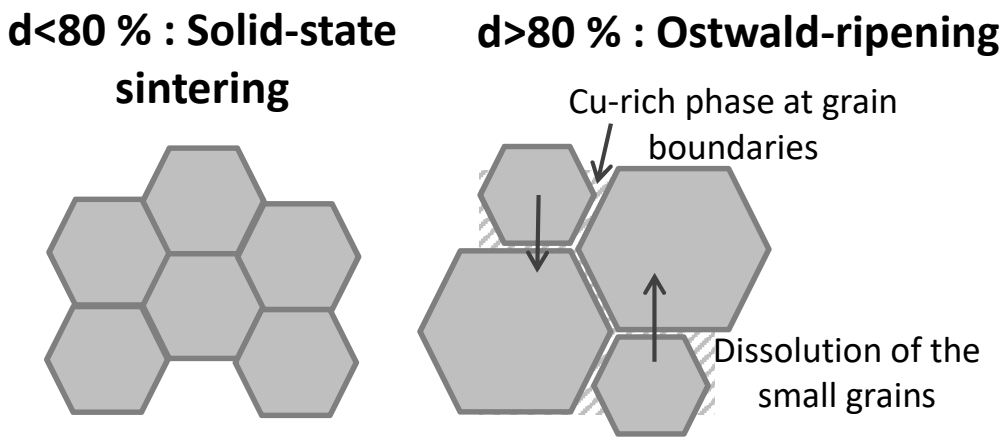

Figure 8: Scheme of the proposed grain growth mechanism in CCTO.